Investigation of the correlation between the electrical contact resistance and the contact area of mechanical lap joint fabricated with high-temperature superconducting tapes using X-ray microtomography

Investigation of the Correlation between the Electrical Contact Resistance and the Contact Area of Mechanical Lap Joint Fabricated with High-Temperature Superconducting Tapes Using X-ray Microtomography

Weixi Chen, Satoshi Ito, Noritaka Yusa, Hidetoshi Hashizume

Keyword: High-temperature superconducting magnet, Joint-winding, Contact resistance, Non-destructive evaluation, X-ray Computer Tomography scan, Image segmentation

Abstract

A mechanical lap joint fabricated with high-temperature superconducting (HTS) tapes is proposed for the application to joint-winding in HTS magnets for fusion reactors. The applicability of the joint has been validated, however, it could not be guaranteed because the joint resistance is unpredictable before the entire conductor is cooled and energized. Identifying the factors that affect the joint resistance is necessary to develop a method to predict this parameter at room temperature. In this report, we evaluated the correlation between the electrical resistance of contact interfaces (contact resistance) and the contact area observed using X-ray computer tomography scan (observed contact area), and discussed appropriate techniques for this prediction. A total of 40 mechanical lap joint samples were prepared. The observed contact areas were segmented from cross-sectional images of contact interfaces using a graph cut image segmentation, while the contact resistances were calculated from measured joint resistances. The correlation indicated that the prediction of contact resistance is more precise when base on the observed contact area compared to the conventional method using the nominal contact area. However, some of dispersive contact resistivity still remained due to inhomogeneous distribution of fine-structure on contact interface.

1. Introduction

"Remountable" (demountable) high-temperature superconducting (HTS) magnets [1-8] with coil segments that are mounted and demounted repeatedly using mechanical joints is proposed for advanced heliotoron-type and compact tokamak fusion reactors. The joint-winding concept [8-10], where a coil is wound by connecting half- or single-pitch HTS helical conductor segments using mechanical joints was suggested for the large helical device (LHD)-type fusion reactors, FFHR series in particular [11] [12]. Considering the current viable fabrication techniques, the joint-winding is the primary option for constructing helical coils, whereas the remountable magnet is an advanced option. Ohmic-heating generated from non-superconducting materials at the joint section can be tolerated by using HTS materials with larger heat capacity and higher temperature margin compared to low-temperature superconducting materials. Among the potential HTS wires and tapes, rare-earth barium copper oxide (REBCO) tape is an ideal candidate because of its high current density under high magnetic fields, high mechanical strength, and low radioactivation.

For joint-winding, Stacked Tapes Assembled in Rigid Structure (STARS) conductor [10], where simply-stacked REBCO tapes are embedded in copper and stainless-steel jackets have been proposed for use in helical-shaped conductor segments with easy-fabricable resistive lap joints. Several types of resistive lap joint have been studied for various HTS applications. Solder joint with tin-lead solder has achieved joint resistivity (the product of the joint resistance and the nominal contact area) of 2-5 pΩm^2 at 77 K, self-field [13-15]. However, tin-lead solder has a risk to decrease critical current (I_c) due to the temperature limit of HTS material without oxygen annealing in a large-scale conductor, which has ununiformed heating temperature distribution and prolonged heating time during heat process. Nano-particle metal paste joint is one example not require oxygen annealing, and it realized 4.8 pΩm^2 with 1 hour heat treatment [16]. One candidate to shorten the joining process is ultrasonic welding (UW) [17]. Combined UW technique with solder realized 5.7 pΩm^2 [18]. Considering repeatedly fabrication and demount ability of joint, we developed mechanical lap joint where REBCO tapes are pressed together with indium foil inserted in-between the tapes. A joint resistivity of 5 pΩm^2 has been achieved with the joint fabricated at room temperature [19], and was able to be improved to 2.5 pΩm^2 with low-temperature heat treatment at about 100 degree C [20] [21]. The mechanical lap joint is now the first candidate for the joint-winding because of sufficiently low joint resistance, simple fabrication process and applicability to large-scale joint. In a previous study [22], we applied bridge-type mechanical lap joint with indium (with no heat treatment) to a large-scale conductor and succeeded in achieving a joint resistance of 1.8 nΩ (corresponding to 10 pΩm^2). This was achieved with 100 kA energizing at 4.2 K, 0.45 T using a STARS conductor with 3-row and 14-layer of 10-mm-wide REBCO tape and the joint resistance achieved by the bridge-type joint was sufficiently low from the perspective of cooling power. However, the joint resistance could only be evaluable after cooling, and energizing because of the difference in the current path between the

ambient and cryogenic environments at the joint. This situation is not desirable; the helical coil is constructed with 7800 joints using half-pitch segments [11]. An inspecting and qualification technique at room temperature is indispensable to realize a reliable fabrication process for these joints.

In this regard, we indevoured to identify the factors that affect joint resistance in the development of an appropriate prediction technique. Joint resistance involves the electrical resistances from non-superconducting materials and the contact interface between the REBCO tape and indium (contact resistance). The contact resistance is estimated by subtracting the experimentally measured joint resistance from the resistances of the non-superconducting materials. The estimated contact resistance depends on the size of the contact area used to calculate the resistance of the non-superconducting materials. In a conventional evaluation, the "nominal contact area S_n," which is calculated simply by multiplying the joint length and width of the REBCO tape is used to calculate contact resistance. However, the actual contact area inside the joint should be utilized. X-ray computer tomography (CT) scan is known for its excellent nondestructive inner inspection ability. It was used for analyzing condition of filament in superconducting material [23] [24], and tracing trajectories of superconducting wires in Cable-in-Conduit Conductor (CICC) [25]. As a pioneer to introduce this technology for analyzing joint, our earlier study [26] has used X-ray CT scan to observe the contact interfaces to evaluate the area or to analyze the contact condition inside the joint. It was determined that there were random gaps at the contact interfaces. In this study, the influence of these gaps on the joint resistance was quantitatively evaluated. Specifically, 40 mechanical lap joint samples were prepared. X-ray CT scan was used initially used to acquire and analyze cross-sectional images of contact interfaces. The observed contact area was denoted as "observed contact area S_{CT}." The joint resistance of each sample was then measured. Subsequently, the contact resistance was estimated using the measured joint resistance and two contact areas, S_n and S_{CT}. Finally, the correlation between each contact area and the estimated contact resistance was evaluated. The development of a predicting technique for joint resistance is discussed in this work based on the analysis of the evaluated contact area and resistance.

2. Materials and Methods

2.1 Sample Preparation

The samples were mechanical lap joints with 4-mm-wide copper-stabilized REBCO tapes (SCS4050-AP, SuperPower Inc, Schenectady, NY, USA, I_c : over 91 A at 77 K and self-field). The tapes from two different lots were used, and denoted as lot A and lot B. The compositions and the thickness of the tapes: the layers from top to bottom are: copper (20 μm), silver (1.6 μm), REBCO (1.6 μm), buffer layers (less than 0.2 μm), Hastelloy substrate (50 μm), silver (1.6 μm), and copper (20 μm). The copper layer at the top of the tapes at the joint section was polished using sandpaper (the diameter of the abrasive particle was 81 μm) and then cleaned with ethanol. The thickness of the indium foil was originally 100 μm and the surface of the indium was also cleaned using ethanol. After polishing and cleaning, the tops of the two tapes at the joint area were set face-to-face and the indium foil was inserted between them. The joint area was then pressed together with a joint pressure of 100 MPa at room temperature (approx. 293 K) for 1 minute. The thickness of the joint was measured using a micrometer after the release of the pressure because indium deformed plastically during the pressing process. We prepared 40 samples: 22 samples using REBCO tapes from lot A, of which 14 samples had a 5 mm joint length, 4 samples had a 2 mm joint length, and 4 samples had a 10

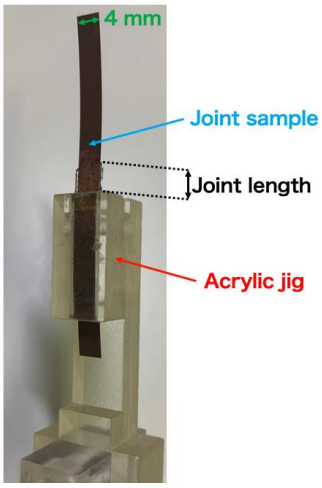

Fig. 1 Sample set for X-ray CT scan

mm joint length. For the 18 samples using the REBCO tapes from lot B, all their joint length was 5 mm.

2.2 Contact area evaluation

Each sample was set in an acrylic jig as shown in Fig. 1 and inspected using micro X-ray CT scanner (ScanXmate-D160TS110, Comscantecno Company Ltd., Yokohama, Japan) to observe two interfaces between the REBCO tapes and the indium foil. The number of projections was 600, and the X-ray tube voltage and X-ray tube current were set to be 145 kV and 20 μA, respectively. A metallic filter was not used. The obtained three-dimensional CT data consists of 496×496×496 voxels. The size of the voxel was 13.168 μm for the samples with 2 mm and 5 mm joint length, and 25.957 μm for 10 mm long joint samples, which were the smallest for the sizes of sample and the X-ray tube conditions.

Figure 2 shows schematic cross-sectional images of the contact interfaces. After the acquisition of the three-dimensional data, the area of two REBCO tapes superposing was identified as the region of interest (ROI) based on X-ray transmission images of the joint. This is because a preliminary numerical simulation to evaluate current distribution indicated that the indium outside the superposing area has little effect on the joint resistance. Then we manually extracted two-dimensional cross-sectional images corresponding to the contact interfaces shown in Fig. 2 (b). In order to reduce the computational resource necessary for subsequent image segmentation, Simple Linear Iterative Clustering [27] was applied to the extracted images. The number of superpixel was 5120. Subsequently, graph cut was utilized [28] to segment the ROI into areas with and without gaps because a preliminary numerical simulation of X-ray CT scan confirmed that only the presence of air contributes to an abrupt change in the CT number. Points with a locally small CT number were chosen as initial seeds for areas with gaps; those with a relatively large CT number were choose as the areas of the observed contact area. Finally, the calculation was executed and the two observed contact areas of the two contact interfaces are denoted as S_{CT1} and S_{CT2}. To enhance the visibility of the ROI and the seeds of the gap areas, the contrast of the image was appropriately adjusted using histogram equalization and segmentation processing was performed three times to evaluated the error caused by the different initial seed points. All image segmentations were performed using MATLAB R2018a with the Image Processing Toolbox.

Samples were inspected by X-ray CT scan before and after the resistance measurement described in 2.3 to confirm the validity of discussing the effect of contacts areas on contact resistances at cryogenic state.

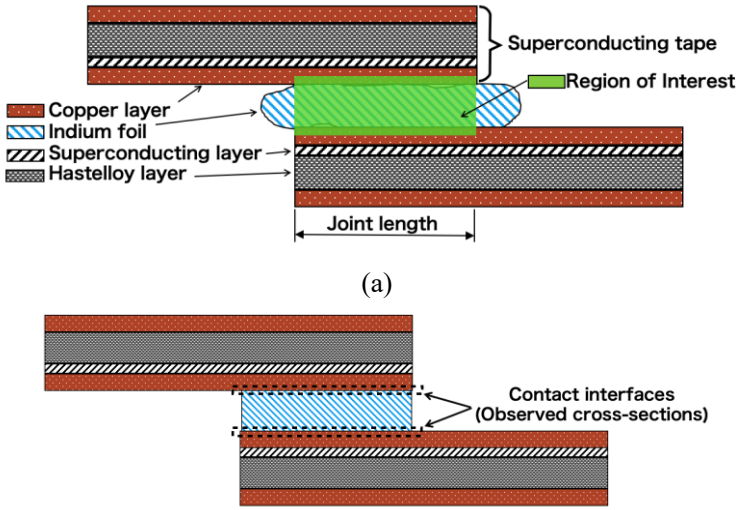

Fig. 2 Configuration of extracted cross-sectional images: (a) Region space of ROI (b) Positions of observed cross-sections at joint

2.3 Contact resistance evaluation

After acquiring X-ray CT scan, each sample was cooled using liquid nitrogen (77 K) and the joint resistance, R_{joint}, was measured from the current-voltage slope (I-V curve) using the four-terminal method. The two terminals that were used to measure voltage were set on both REBCO tapes that straddle the joint, with a separation distance of approximately 20 mm. Currents up to 40 A (0, 10, 20, 30, and 40 A) were applied, and the joint resistance was evaluated by applying the least squares approach to the measured I-V curve. Each sample was soaked into liquid

nitrogen, measured twice, and heated to room temperature to confirm reproductivity of the *I-V* curve.

Figure 2 suggests that it is reasonable to model the joint resistance, R_{joint}, as the sum of the resistance of the silver layers, copper layers, and indium foil, in addition to the interface resistance inside the REBCO tapes and contact resistances at the two contact interfaces. The sum of two contact resistances as evaluated using a conventional method, R_n, can be expressed as

$$R_n = R_{joint} - \left(2 \times \rho_{Ag} \frac{T_{Ag}}{S_n} + 2 \times \rho_{inter} \frac{1}{S_n} + 2 \times \rho_{Cu} \frac{T_{Cu}}{S_n} + \rho_{In} \frac{T_{In}}{S_n}\right) \quad (1)$$

where ρ_{Ag}, ρ_{Cu}, ρ_{In}, are the resistivities of silver, copper, and indium at 77 K (ρ_{Ag}=2.70×10^{-9} Ωm, ρ_{Cu}=2.10×10^{-9} Ωm, ρ_{In}=1.67×10^{-8} Ωm) [29], T_{Ag}, T_{Cu}, T_{In} are the thicknesses of silver, copper, and indium, and T_{in} was in 32 μm to 94.5 μm range. ρ_{inter} (= 1.05 pΩm^2) is the interface resistivity determined from a previous study [30]. For the observed contact areas, the sum of two contact resistances, R_{CT}, can be expressed as

$$R_{CT} = R_{joint} - \left(\rho_{Ag} \frac{T_{Ag}}{S_{CT1}} + \rho_{inter} \frac{1}{S_{CT1}} + \rho_{Cu} \frac{T_{Cu}}{S_{CT1}} + \rho_{In} \frac{T_{In}}{\sqrt{S_{CT1}}\sqrt{S_{CT2}}} + \rho_{Cu} \frac{T_{Cu}}{S_{CT2}} + \rho_{inter} \frac{1}{S_{CT2}} + \rho_{Ag} \frac{T_{Ag}}{S_{CT2}}\right) \quad (2)$$

Each contact resistance was calculated using equation (1) and (2), respectively.

3. Results and discussion

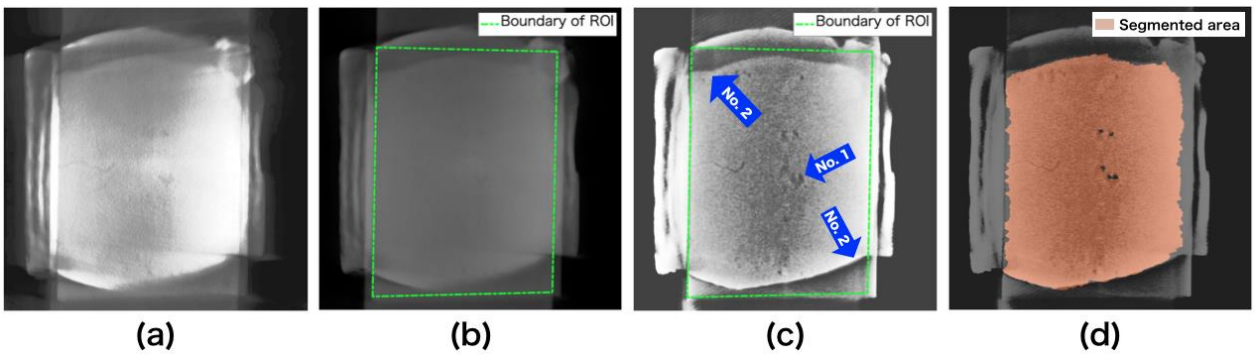

Fig. 3 Segmentation process for cross-section images: (a) X-ray transmission image of joint with adjusted contrast, (b) Ranged ROI of joint, (c)Cross-sectional images of contact interface with adjusted contrast, (d)Segmented contact area

A series of image segmentation is introduced in Fig. 3. Figure 3 (a) represents the X-ray transmission image of a sample with a joint resistance of 0.279 μΩ (corresponding to a joint resistivity of 5.58 pΩm^2) and its ROI was the ranged following the contour of the tapes as shown in Fig. 3 (b). Figure 3 (c) shows one of the two cross-sectional images of the two contact interfaces from the sample which were extracted from the X-ray CT data. It should be noted that the shape of the two REBCO tapes in Fig. 3 (c) consists of the top surface of the REBCO tape and a partial volume averaging, which is a kind of artifact of X-ray CT. In Fig. 3 (c), the dark areas around the center of the joint were identified as gap areas. The seeds of the gap were chosen at these spots (arrowhead No. 1). In addition, a discontinuous and dark area in the upper and lower area in the ROI could be observed (arrowheads No. 2). These are dark bands, which is another kind of artifact of X-ray CT, caused by the boundary between different X-ray attenuation properties. The seeds of the gap area were also selected in these dark bands areas. The seeds of the observed contact area were selected at the area except for the gap areas as arrowhead No. 1 and No. 2. The calculation of graph cut was executed and Fig. 3 (d) shows the segmented observed contact area acquired from the cross-sectional image.

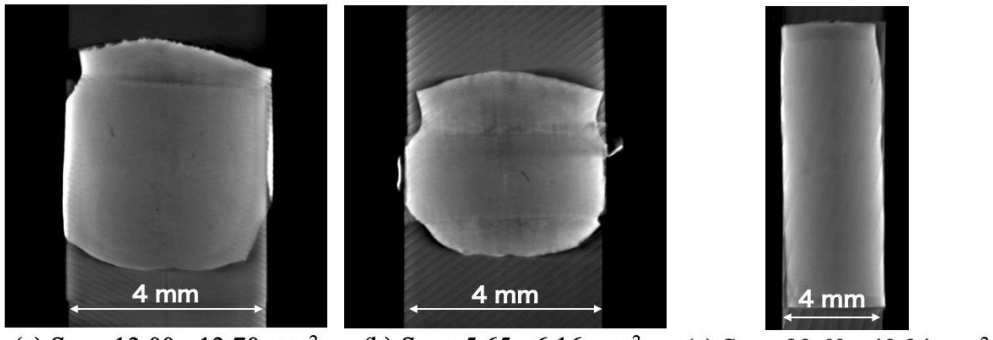

(a) S_{CT1}=13.00 - 13.70 mm^2 (b) S_{CT1}=5.65 - 6.16 mm^2 (c) S_{CT1}=39.60 - 40.94 mm^2

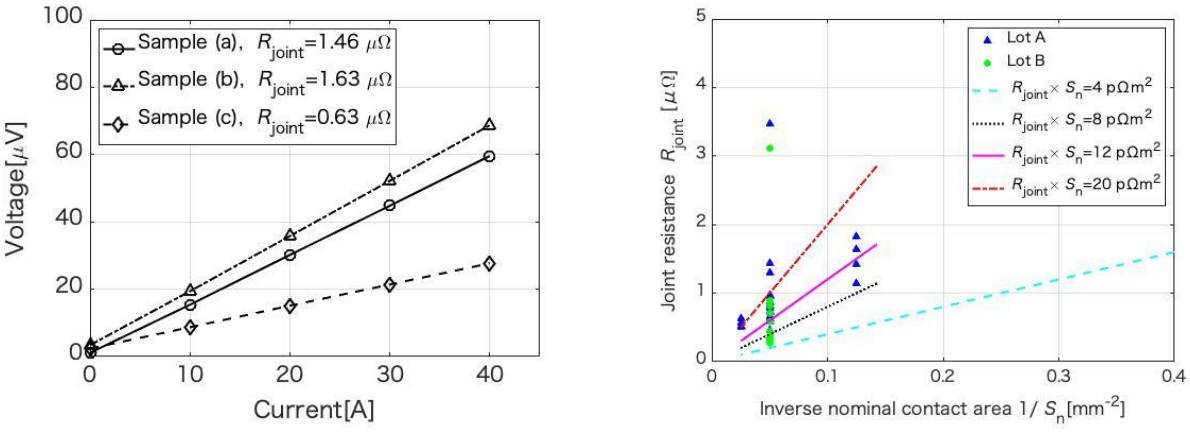

(d) (e)

Fig. 4 Experimental result, Cross-sectional image of one contact interface from joint sample with (a) 5 mm joint length, (b) 2 mm joint length, (c) 10 mm joint length, (d) three representative samples and corresponding measured *I-V* curve (e) Relationship between joint resistance and inverse nominal contact area.

Examples of the measured experimental result is shown in Fig. 4. Figure 4 (a), (b), (c) represent one cross-sectional image of two contact interfaces from samples with joint lengths of 2 mm, 5 mm, and, 10 mm, respectively. The area of the smallest gap indicated by the procedure described in 2.2 was 5.38×10^{-3} mm^2. The change rate of evaluated contact area before cooling and after cooling is –2.48% in average. Four of 40 samples varied ±10% in and the maximum variation was –17.62%. Since the image processing here revealed that manually choosing the seeds led error in evaluating contacted area, and the majority of samples varied slightly, we considered the cooling did not affect the observed contact area significantly. The *I-V* curves and calculated joint resistances R_{joint} corresponding to the samples of (a), (b), (c) are shown in Fig. 4 (d), and the relationship between R_{joint} and inverse nominal contact area S_n of all samples were shown in Fig. 4 (e). The minimum joint resistivity of the sample was 4 pΩm^2 in conventional evaluation.

The relationship between the contact resistances R_n and the sum of two inverse nominal contact areas $2/S_n$ is shown in Fig. 5 (a). The lines correspond to contact resistivities of 4, 8, 12, and 20 pΩm^2. This parameter is calculated by multiplying the contact resistance R_n and the sum of the two nominal contact areas $2\times S_n$ to determine the average contact condition of the two contact interfaces. The results indicate that except for the two samples enclosed by the dot-lines which had relatively high contact resistance, the sample with larger contact areas tended to have relatively high contact resistivity. We considered that the existence of gaps mainly increased the contact resistivity because of the difficulty of uniformizing joint pressure for larger joints. To verify this assumption, it was necessary to evaluate and eliminate the gap area. In Fig. 5 (b), the relationship between R_{CT} and the sum of the inverse observed contact areas $1/S_{CT1}+1/S_{CT2}$ was shown. The lines correspond to contact resistivities of 4, 8, 12, and 20 pΩm^2 that were determined by multiplying the contact resistance R_{CT} and the sum of the two observed contact area $S_{CT1}+S_{CT2}$. Compare to the result shown in Fig. 5 (a), it was determined that the dependency of contact resistance on contact area tended to be more linear. In particular, the results for samples with a smaller contact area indicates that the contact resistivity are tends to follow same line with a contact resistivity of 4 pΩm^2. The evaluation of the contact condition,

i.e., contact resistivity, produce an accuracy with the elimination of the gap area.

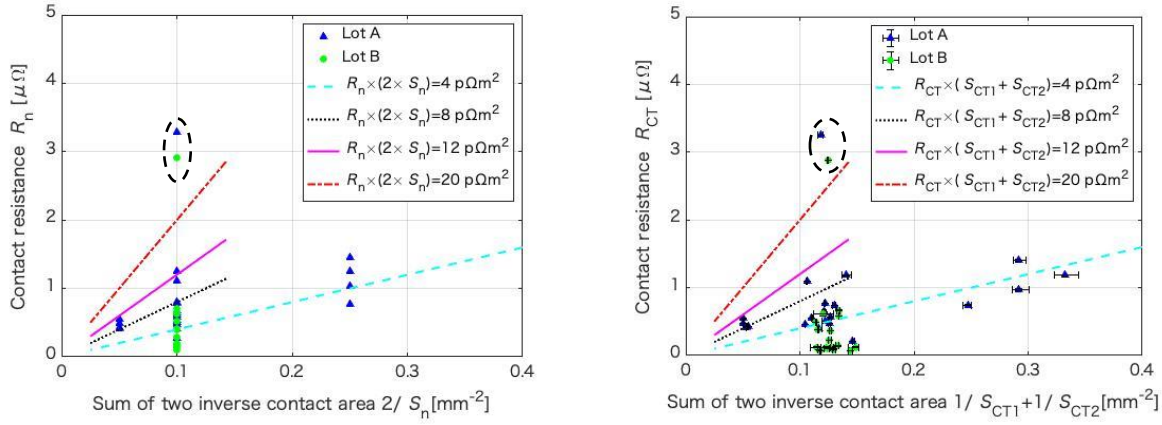

(a) (b)

Fig. 5 Relationship between contact area and contact resistance: (a)Relationship between $2/S_n$ and R_n (b) Relationship between $1/S_{CT1}+1/S_{CT2}$ and R_{CT}

Considering the dispersion of the contact resistivity in Fig. 5 (b), the local critical current degradation on REBCO tapes and the contact condition changes with the scale smaller than X-ray CT resolution are primary causes. For the former, the result without specific difference in the contact resistance based on a comparison of different lots indicated the local degradation might be caused by joining process. In this situation, the flux-flow resistance would be counted together as the contact resistance, resulting in an increment of the contact resistivity. Since the REBCO tapes superposing at the joint were inaccessible using the four-terminal method, we could not examine the quality of the REBCO tapes to eliminate this possibility. For the latter, in the boundary of two different metals, micro-gap, oxidized film and alloy are present. Theoretically, a study [31] showed the real contact area accounts for nominal contact area less than 50% from microscopic-scale point of view. Since the effect of micro-gap and thin oxidized film is too small to affect CT number, and the alloy of the two metals is too similar to be segmented from the other voxels consisting of the same metals. As such, it is difficult to identify the distribution of these micro-order fine structures to evaluate real contact area. In the case that the real contact area distributed uniformly on the $S_{CT1}+S_{CT2}$, we could expect the contact resistance R_{CT} proportional to the inverse contact area $1/S_{CT1}+1/S_{CT2}$. Consequently, the result with dispersive contact resistivity can be interpreted as inhomogeneous distribution of real contact area. Therefore, further studies are needed to clarify the specific distribution of inhomogeneous fine structure, which are finer than the voxel size of X-ray CT scan.

According to the theory of electric contacts [32] and the improvement of the joining method [7] [8] [20] [21] [33] developed based on the theory, the distribution of real contact area varies with the joining process. Based on the aforementioned result, we conclude that the range of the contact resistance prediction is improved with the acquisition of the observed contact area, but cannot be perfectly predicted only from the scale of this region. The condition of the joining process which affects the fine structure of the contact interface also needs to be considered in the prediction of joint resistance.

4. Conclusion

In this study, we evaluated the correlation between the contact area and contact resistance of the mechanical lap joint of REBCO tapes. X-ray CT scan were used to extract cross-sectional images of the contact interfaces. The observed contact area was quantitatively segmented, then the joint resistance was measured, followed by the calculation of the contact resistance. Compared to the relationship between nominal contact area and contact resistance using a conventional method, the relationship between the observed contact area with contact resistance reflected more accurate contact resistivity by eliminating the gap area in the joint. This indicated the contact resistance can be predicted more precisely using the observed contact area. However, the local degradation of REBCO tape and micro-order fine structure in the observed contact area is considered to account for dispersive contact resistance. Therefore, depending only on the observed contact area is not appropriate for predicting joint resistance; the joining process is also needed to be considered.

Acknowledgement
This work was supported by JSPS Grants-in-Aid for Scientific research (S) Grant Number 26220913 and Grants-in-Aid for JSPS research Fellow Grant Number 17JD2122. The authors are appreciative of the assistance of associate professor Keitaro Hitomi (Department of Quantum Science Engineering, Tohoku University) for providing technical and hardware support for X-ray spectrum measurements in conducting preliminary simulations of X-ray CT scan. The X-ray CT scan equipment was supported by Tohoku University Microstructural Characterization Platform in Nanotechnology Platform project sponsored by the Ministry of Education, Culture Sports, Science and Technology (MEXT), Japan. We would like to thank Editage (www.editage.jp) for English language editing.

Reference

[1] L. Bromberg, M. Tekkula, L. A. El-Guebaly, R. MIller, and ARIES Team, "Options for the use of high temperature superconductor in Tokamak fusion reactor designs," Fusion Eng. Des., vol. 54, no. 2, pp. 167-180, Feb. 2001.

[2] H. Hazhisume, S. Kitajima, S. Ito, K. Yagi, U. Usui, Y. Hida, A. Sagara, "Advanced fusion reactor design using remountable HTc S. C. magnet," J. Plasma Fusion Res. SERIES., vol. 5, pp. 532-536, 2002.

[3] S. Ito and H. Hashizume, "Overview of fundamental study on remoutable HTS magnet," Fusion Eng. Des., Vol. 81, no. 22, pp. 2527-2533, Nov. 2006.

[4] Z. S. Hartwig, C. B. Haakonsen, R. T. Mumgaard, and L. Bromberg, "And initial study of demountable high-temperature superconducting toroidal field magnets for the Valcan tokamak conceptual design," Fusion Eng. Des., vol. 87, no. 3, pp. 201-214, Mar. 2012.

[5] B. N. Sorbom, J. Ball, T. R. Palmer, F. J. Mangiarotti, J. M. Sierchio, P. Bonoli, C. Kasten, D. A. Sutherland, H. S. Barnard, C. B. Haakonsen, J. Goh, C. Sung, D. G. Whyte, "ARC: A compact, high-field, fusion nuclear science facility and demoustration power plant with demoutable magnets," Fusion Eng. Des., vol. 100, pp. 378-405, Nov. 2015.

[6] H. Hashizume, S. Ito, "Design prospect of remountable high-temperature superconducting magnet," Fusion Eng. Des., vol. 89, no. 9-10, pp. 2241-2245, Oct. 2014.

[7] H. Hashizume, S. Ito, N. Yanagi, H. Tamura and A. Sagara, "Development of remountable joints and heat removable techniques for high-temperature superconducting magnets," Nucl. fusion, vol. 58, no. 8, 026014, Dec. 2017.

[8] S. Ito, H. Hashizume, N. Yanagi, T. Tamura, "Advanced high-temperature superconducting magnet for fusion reactors: Segment fabrication and joint technique," Fusion Eng. Des., vol. 136, part A, pp. 239-246, Nov. 2018.

[9] N. Yanagi, T. Mito, R. Champailler, G. Bansal, H. Tamura, A. Sagawa, "Design progress on the high-temperature superconducting coil option for the heliotron-type fusion energy reactor FFHR," Fusion Sci. Technol., vol 60. no. 2, pp. 648-652, Aug. 2011.

[10] N. Yanagi, S. Ito, Y. Terazaki, Y. Seino, S. Hamaguchi, H. Tamura, J. Miyazawa, T. Mito, H. Hashizume and

A. Sagara, "Design and development of high-temerature superconducting magnet system with joint-winding for the helical fusion reactor," Nucl. fusion, vol. 55, no. 5, 053021, Apr. 2015.

[11] A. Sagara, H. Tamura, T. Tanaka, N. Yanagi, J. Miyazawa, To. Goto, R. Sakamoto, J. Yagi, T. Watanabe, S. Takayama, the FFHR design group, "Helical reactor design FFHR-d1 and c1 for steady-state DEMO," Fusion Eng. Des., vol. 89, no. 10, pp. 2114-2120, Oct. 2014.

[12] A. Sagara, J. Miyazawa, H. Tamura, T. Tanaka, T. Goto, N. Yanagi, R. Sakamoto, S. Masuzaki H. Ohtani and The FFHR Design Group, "Two conceptual designs of helical fusion reactor FFHR-d1A based on ITER technologies and challenging ideas," Nucl. fusion, vol. 57, no. 8, 086046, Jul. 2017.

[13] J. Lu, K. Han, W. R. Sheppard, Y. L. Viouchikov, K. W. Pickard, and W. D. Markiewicz, "Lap Joint resistance of YBCO Coated Conductors," IEEE Trans. Appl. Supercond, vol. 21, no. 3, 3009, Jun. 2011.

[14] R. Tediosi, M. Alessandrini, C. Beneduce, S. Scheneider, and D. Eckert, "Low Temperature and Magnetic Field Performance of Spliced Commercial YBCO CC," IEEE Trans. Appl. Supercond., vol. 22, no. 3, 6600804, Jun. 2012.

[15] N. Bagrets, A. Augieri, G. Celentano, G. Tomassetti, K. Weiss, and A. della Corte, "Investigation of ReBCO Conductor Tape Joints for Superconducting Applications," IEEE Trans. Appl. Supercond., vol. 25, no. 3, 6602705, Jun 2015.

[16] T. Nakanishi, T. Machi, T. Izumi, R. Teranishi, T. Kato, T. Kato and T. Hirayama, "Jointing of Coated Conductors by Using Nano-particle Metal Pastes," Phys. Procedia, vol. 81, pp. 105-108, 2016.

[17] H. S. Shin, J. M. Kim, "Parametric Study for Low-Resistance Joint of REBCO Coated Conductor Tapes Using Ultrasonic Welding," IEEE Trans. Appl. Supercond. vol. 26, no. 3, 6603205, Apr. 2016.

[18] H. S. Shin, J. M. Kim and M. J. Dedicatoria, "Pursuing Low Joint Resistivity in Cu-stabilized ReBa2Cu3Oδ Coated Conductor Tape by The Ultrasonic Weld-solder Hybrid Method," Supercond. Sci. Techno. vol. 29, 015005, 9pp, 2016.

[19] K. Kawai, S. Ito, T. Seino, N. Yanagi, H. Tamura, A. Sagara, H. Hashizume, "Optimization of a mechanical bridge joint structure in a stacked HTS conductor," IEEE Trans. Appl. Supercond., vol. 23, no. 3, 6409408, Jun. 2013.

[20] T. Nishio, S. Ito, N. Yusa, and H. Hashizeme, "Reducing Joint Resistance by Heat Treatment During Fabrication of a Mechanical Joint of High-Teperature Superconducting Conductors," IEEE Trans. Appl. Supercond.,vol. 26, no. 4, 4800505, Jun. 2016.

[21] T. Nishio, S. Ito, H. Hashizume, "Heating and loading process improvement for indium inserted mechanical lap joint of REBCO rapes," IEEE Trans. Appl. Supercond. vol. 27, no. 4, 4603305, Jun. 2017.

[22] S. Ito, Y. Seino, N. Yanagi, Y. Terazaki, A, Sagara, H. Hashizume, "Bridge-type mechanical lap joint of a 100

kA-class HTS conductor having stacks of GdBCO tapes," Plasma Fusion res., vol. 9, 3405086, Jun. 2014.

[23] C. Scheuerlein, M. Di. Michiel, M. Scheel, J. Jiang, F. Kametani, A. Malagoli, E. E. Hellstrom and D. C. Lardalestier, "Void and phase evolution during the processing of Bi-2212 sueprconducting wires monitored by combined fast synchrotron mictro-tomography and X-ray diffraction," Supercond. Sci. Technol. vol. 24, No. 11, 115004, Sept. 2011..

[24] M. Inoue, H. Tartara, K. Harada, K. Higashikawa, S. Ye, A. Matsumoto, H. Kumakura, and T. Kiss, "Three-Demensional Analysis of MgB2 Wire by use of X-ray Micro-Tomography," IEEE Trans. Appl. Supercond. vol. 26, No. 3, 6201004, Apr. 2016..

[25] I. Tiseanu, L. Zani, T. Craciunescu, F. Cotorobai, C. Dobrea, A. Sima, "Characterization of superconducting wires and cables by X-ray micto-tomography," Fusion Eng. Des., vol. 88, pp. 1613-1618, Mar. 2013.

[26] S. Ito, N. Yusa, N. Yanagi, H. Tamura, A. Sagara, H. Hashizume, "Mechanical and electrical characteristics of a bridge-type mechanical lap joint of HTS STARS conductors," IEEE Trans. Appl. Supercond., vol. 26 no 2, March 2016.

[27] R. Achanta, A. Shaji, K. Smith, A. Lucchi, P. Fua, S. Süsstrunk, "SLIC Superpixels Compared to State-of-the-art Superpixel Methods," IEEE Trans. Pattern. Anal. Mach. Intell., Vol. 34, 11, pp2274-2282, Nov. 2012.

[28] C. Rother, V. Kolmogorov, A. Blake, ""GrabCut" - Interactive Foreground Extraction using Iterated Graph Cuts," ACM Trans. Graph., vol. 23, 3, pp. 309-314, Aug. 2004.

[29] J. W. Ekin, Experimental Techniques for Low-Temperature Measurements, Boulder, Colorado: Oxford univ. Press, 2006.

[30] R. Hayasaka, S. Ito, H. Hashizume, "Evaluation of Interface Resistance in a REBCO Tape at Different Temperatures by Contact -probing Current Transfer Length Method," IEEE Trans. Appl. Supercond., in press, 2019.

[31] J. B. P. Williamson and R. T. Hunt, "Asperity persistence and the real area of contact between rough surfaces," Proc. R. Sox. Lond. A. vol. 327, 147-157, Mar. 1972.

[32] R. Holm, Electric Contacts Theory and Application, New York, NY, USA: Spring-Verlag, 1967.

[33] S. Ito, H. Hashizume, N. Yanagi, H. Tamura, "Bridge-type mechencanical lap joint of HTS STARS conductors using an integrated joint piece," Fusion Eng. Des., in press, 2019.